Check for updates

Received: 29 August 2025 | Revised: 13 October 2025 | Accepted: 17 October 2025

DOI: 10.1002/pro.70362

RESEARCH ARTICLE

THE PROTEIN SOCIETY WILEY

Structures of two LarA-like nickel-pincer nucleotide cofactor-utilizing enzymes with a single catalytic histidine residue

Santhosh Gatreddi[1,2] | **Sundharraman Subramanian**[2] | **Dexin Sui**[2] | **Tianqi Wang**[2] | **Julian Urdiain-Arraiza**[3] | **Benoît Desguin**[3] | **Robert P. Hausinger**[1,2] | **Kristin N. Parent**[2] | **Jian Hu**[2,4]

[1]Department of Microbiology, Genetics, and Immunology, Michigan State University, East Lansing, Michigan, USA

[2]Department of Biochemistry and Molecular Biology, Michigan State University, East Lansing, Michigan, USA

[3]Louvain Institute of Biomolecular Science and Technology (LIBST), Université catholique de Louvain, Louvain-La-Neuve, Belgium

[4]Department of Chemistry, Michigan State University, East Lansing, Michigan, USA

Correspondence
Robert P. Hausinger, Department of Microbiology, Genetics, and Immunology, Michigan State University, East Lansing, MI, USA.
Email: hausinge@msu.edu

Kristin N. Parent and Jian Hu, Department of Biochemistry and Molecular Biology, Michigan State University, East Lansing, MI, USA.
Email: kparent@msu.edu and hujian1@msu.edu

Funding information
UCLouvain Fonds Spécial de Recherche; National Institutes of Health, Grant/Award Numbers: GM128959, GM140803, GM140931

Review Editor: Jeanine Amacher

Abstract

The nickel-pincer nucleotide (NPN) cofactor catalyzes the racemization/epimerization of α-hydroxy acids in enzymes of the LarA family. The established proton-coupled hydride transfer mechanism requires two catalytic histidine residues that alternately act as general acids and general bases. Notably, however, a fraction of LarA homologs (LarAHs) lack one of the active site histidine residues, replacing it with an asparaginyl side chain that cannot participate in acid/base catalysis. Here, we investigated two such LarAHs and solved their cryo-electron microscopic structures with and without loaded NPN cofactor, respectively. The structures revealed a consistent octameric assembly that is unprecedented in the LarA family and unveiled a new set of active site residues that likely recognize and process substrates differently from those of the well-studied LarAHs. Genomic context analysis suggested their potential involvement in carbohydrate metabolism. Together, these findings lay the groundwork for expanding the breadth of reactions and the range of mechanisms of LarA enzymes.

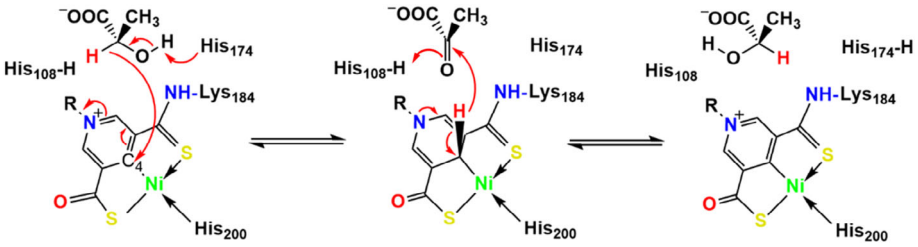
KEYWORDS
cryo-electron microscopy, enzyme, epimerase, LarA, nickel, nickel-pincer nucleotide cofactor, racemase, structure

1 | INTRODUCTION

The organometallic nickel-pincer nucleotide (NPN) cofactor is composed of a nickel ion pincered by two sulfur and one carbon atoms from a pyridinium 3,5-dithiocarboxylate mononucleotide (P2TMN) (Chatterjee, Gatreddi, et al., 2022; Hausinger et al., 2018). The NPN cofactor, first discovered in the lactate racemase, LarA, from *Lactiplantibacillus plantarum* ($LarA_{Lp}$) (Desguin et al., 2015), is biosynthesized by LarB (Chatterjee et al., 2023; Rankin et al., 2021), LarE (Chatterjee, Parson, et al., 2022;

Santhosh Gatreddi and Sundharraman Subramanian contributed equally to this work.

This is an open access article under the terms of the Creative Commons Attribution License, which permits use, distribution and reproduction in any medium, provided the original work is properly cited.
© 2025 The Author(s). *Protein Science* published by Wiley Periodicals LLC on behalf of The Protein Society.



SCHEME 1 $LarA_{Lp}$ catalyzed lactate racemization via a proton-coupled hydride transfer mechanism. Two catalytic residues (His108 and His174) alternately act as general acids/bases. The C4 atom of the nickel-pincer nucleotide cofactor acts as a hydride acceptor during lactate racemization via a pyruvate intermediate. Nickel may also transiently bind the hydride during the racemization reaction.

Fellner et al., 2017, 2018), and LarC (Desguin et al., 2018; Turmo et al., 2022) from nicotinic acid adenine dinucleotide (Desguin et al., 2016), a precursor of nicotinamide adenine dinucleotide (NAD). Lactate racemase catalyzes the interconversion between L- and D-lactate, offering an alternative to NAD-dependent stereospecific lactate dehydrogenases for generating lactate enantiomers involved in diverse biological processes, including cell wall synthesis. Lactate racemization activity has been reported in different bacteria for years (Cantwell & Dennis, 1974; Hiyama et al., 1968; Katagiri et al., 1961; Shapiro & Dennis, 1965), but it was only in 2014 that $LarA_{Lp}$, the founding member of the LarA family, was identified as a nickel-dependent enzyme (Desguin et al., 2014). The crystal structure of $LarA_{Lp}$ in the active state reveals a covalent linkage of the NPN cofactor to a lysine residue via a thioamide bond, and shows the pincered nickel ion with a histidine residue completing the square-planar coordination (Desguin et al., 2015). Situated over the NPN cofactor of $LarA_{Lp}$ are two highly conserved histidine residues (His108 and His174) that function alternately as general acid and base during catalysis, according to the proposed proton-coupled hydride transfer (PCHT) mechanism (Scheme 1) (Chatterjee, Gatreddi, et al., 2022; Desguin et al., 2015; Rankin et al., 2018). Despite large sequence variation, LarA homologs (LarAHs) were thought to operate via the same PCHT mechanism, which has been supported by structural biology studies of representative LarA family members. For the family founding member $LarA_{Lp}$, His108 and His174 bind sulfite, which is a strong competitive inhibitor and also an electron donor that can form a covalent S-C bond with the cofactor (Gatreddi et al., 2023; Rankin et al., 2018). A recent study of a LarAH from *Isosphaera pallida* reported the high-resolution structures in complex with three D-enantiomeric substrates, providing direct evidence supporting the catalytic role of the two histidines (Gatreddi et al., 2025). Bioinformatic analysis has led to the identification of more than 20 LarA subfamilies in prokaryotic species, and the genomic context-guided biochemical study revealed diverse NPN cofactor-dependent racemization/epimerization reactions for various α-hydroxy acids (Desguin et al., 2020). LarAHs from eukaryotic species were also recently reported (Urdiain-Arraiza et al., 2025), indicating the distribution of NPN cofactor-dependent enzymes across the three kingdoms of life. The greatly expanded substrate spectrum unveiled in that study underscores the importance of LarAs in the metabolism of α-hydroxy acids and carbohydrates (Urdiain-Arraiza et al., 2025).

Notably, although most LarAHs possess two catalytic histidine residues that are essential for the PCHT mechanism, the second histidine residue (His174 in $LarA_{Lp}$) in a small fraction of LarAHs is substituted by other amino acids, often an asparagine that cannot function as a general acid/base in catalysis. None of these LarAHs have been characterized, leaving unsolved questions concerning the structure–function relationship and catalytic mechanism of these putative enzymes. In this work, we report the cryo-electron microscopy (cryo-EM) structures of two such LarAHs from *Blautia wexlerae* ($LarA_{Bw}$) and *Streptococcus plurextorum* ($LarA_{Sp}$) in the NPN cofactor-free (apo) and NPN cofactor-loaded (holo) states, respectively, revealing an octameric state and a different active site from the other known LarAHs. Structural analysis, together with genomic context analysis, allowed us to propose their potential involvement in carbohydrate metabolism.

2 | RESULTS AND DISCUSSION

2.1 | Identification of a LarA subfamily with a catalytic histidine-to-asparagine substitution

An early bioinformatic analysis reported three groups of LarAHs that either lack the catalytic histidine residue equivalent to His174 in $LarA_{Lp}$ (Groups 14 and 15) or substitute it with an asparaginyl side chain (Group 17) (Desguin et al., 2020). Using $LarA_{Bw}$ as seed, we conducted a basic local alignment search tool search and identified hundreds of sequences that have an invariable asparagine residue at the position of His174 in $LarA_{Lp}$. Sequence alignment of the selected LarAHs with identity as low as 29% revealed conserved residues in both N- and C-terminal domains (Figure 1),

1469896x, 2025, 12, Downloaded from https://onlinelibrary.wiley.com/doi/10.1002/pro.70362 by Universite Catholique De Louvain, Wiley Online Library on [13/11/2025]. See the Terms and Conditions (https://onlinelibrary.wiley.com/terms-and-conditions) on Wiley Online Library for rules of use; OA articles are governed by the applicable Creative Commons License

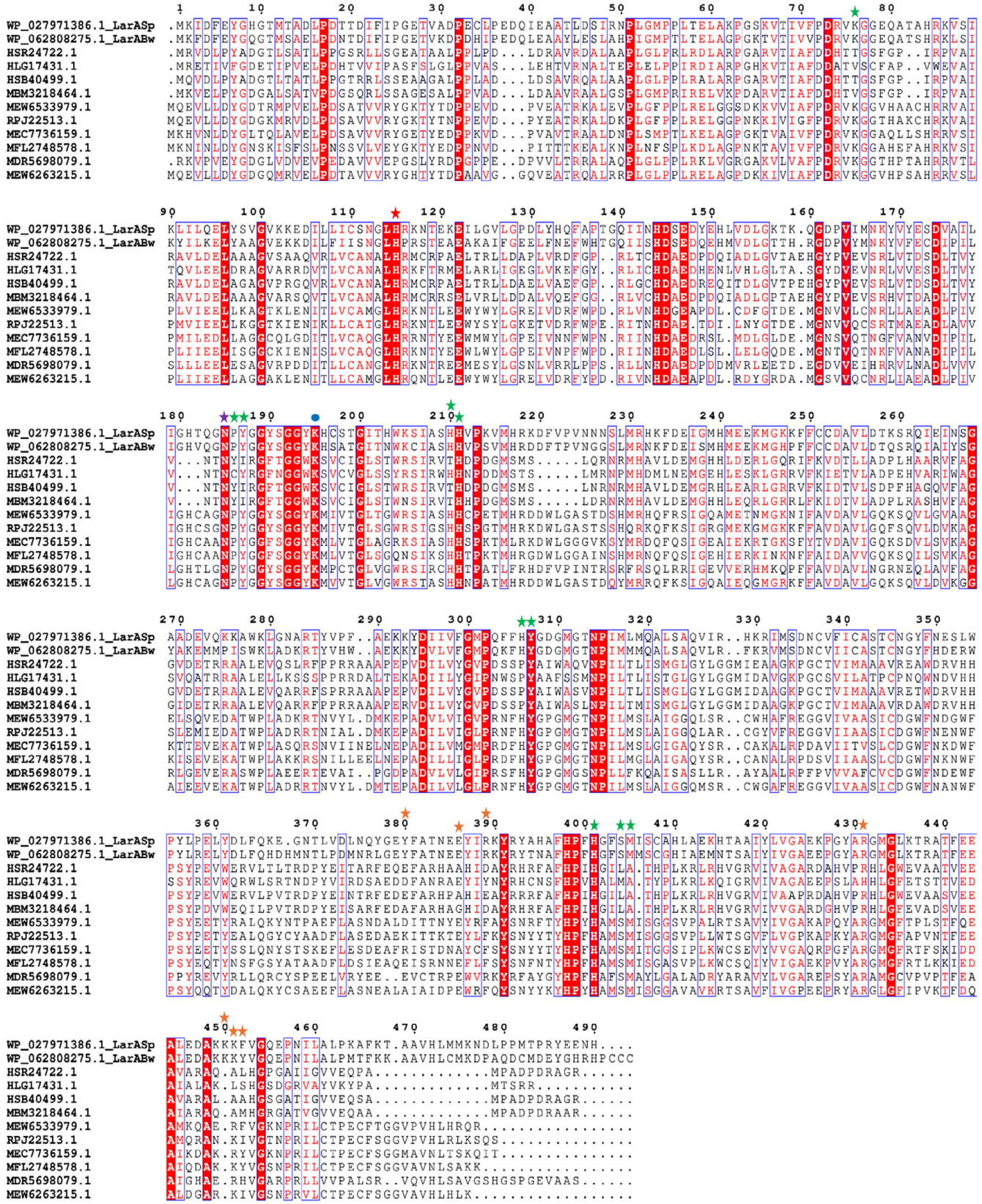


FIGURE 1 Legend on next page.

14698096x, 2025, 12, Downloaded from https://onlinelibrary.wiley.com/doi/10.1002/pro.70362 by Universite Catholique De Louvain, Wiley Online Library on [13/11/2025]. See the Terms and Conditions (https://onlinelibrary.wiley.com/terms-and-conditions) on Wiley Online Library for rules of use; OA articles are governed by the applicable Creative Commons License

which are responsible for the binding of the NPN cofactor and substrate, respectively. Many residues conserved in this group of LarAHs, including the asparagine residue replacing the catalytic histidyl group, differ from those in other LarA subfamilies (Figure S1). Phylogenetic analysis showed that these LarAHs, represented by $LarA_{Bw}$ and $LarA_{Sp}$, form a distinct branch from other LarAHs with known substrates (Figure S2). Thus, these LarAHs likely form a unique subfamily that performs uncharacterized functions.

2.2 | Cryo-EM structure of $LarA_{Bw}$ in the apo state

For structural study, the NPN cofactor is often incorporated in vivo by co-expression with the NPN-synthesizing enzymes (LarB/C/E) in *Lactococcus lactis* (Desguin et al., 2015; Gatreddi et al., 2023, 2025; Rankin et al., 2018). In vivo incorporation with co-expressed Lar proteins in *Escherichia coli* or in vitro incorporation with biosynthesized NPN cofactor is an option for functional study but not recommended for structural study due to the relatively low incorporation efficiency (Desguin et al., 2016, 2020; Nevarez et al., 2024; Urdiain-Arraiza et al., 2025). One protein that we characterized from this newly identified LarA subfamily is a putative enzyme from a commensal human gut bacterium *B. wexlerae*. However, co-expression with the NPN-synthesizing enzymes in *Lactococcus lactis* produced only colorless protein, indicating that the purified $LarA_{Bw}$ is in the apo state because otherwise the LarAH would be yellow or brown due to the NPN cofactor. While it is not uncommon that the NPN cofactor fails to be efficiently incorporated into a LarAH in vivo (Gatreddi et al., 2022), this unsuccessful attempt limited our characterization of $LarA_{Bw}$ to the apo form. For a better yield, the His_6-tagged protein was overexpressed in *E. coli* and purified to homogeneity using immobilized metal affinity chromatography and size exclusion chromatography (SEC) (Figure 2a). Sodium dodecyl sulfate–polyacrylamide gel electrophoresis (SDS-PAGE) indicated a single band consistent with the theoretical molecular weight of 57.5 kDa. Based on the SEC elution profile and comparison to marker proteins, the purified $LarA_{Bw}$ was in a large oligomeric state with an apparent molecular weight of ~360 kDa.

We were unable to crystallize $LarA_{Bw}$, but its structure was readily solved by cryo-EM with a C4 symmetry at a resolution of 3.15 Å, revealing an octameric assembly (Figure 2b,c). Like other LarAHs, $LarA_{Bw}$ is a two-domain protein with the putative active site located between the N- and C-terminal domains (Figure 2d). The Cα root mean square deviation (RMSD) of the monomeric $LarA_{Bw}$ with $LarA_{Lp}$ (PDB 5HUQ, chain B) is 4.2 Å, indicative of a significant structural difference (Figure 2e). Further analysis of the individual domains showed that the N-terminal domains of $LarA_{Bw}$ and $LarA_{Lp}$ could be reasonably aligned with a Cα RMSD of 1.25 Å, whereas the large portion of the C-terminal domains cannot be aligned despite the similar arrangement of the secondary structure elements. The large RMSD of 4.2 Å for the full-length proteins can also be attributed to the different domain orientations—$LarA_{Bw}$ adopts a conformation with the active site more open to the solvent than $LarA_{Lp}$. The detailed comparison of the active sites will be elaborated in a later section.

The basic structural unit of the octamer is a symmetrical dimer in which the C-terminal domain of each protomer contacts through extensive polar interactions (Figure 2f, left panel), burying 1076 $Å^2$ surface area. Most of the polar interactions are mediated by the conserved Arg434 (Figure 1), which uses its guanidinium side chain to form hydrogen bonds with multiple backbone carbonyl oxygen atoms from the other protomer. Several other polar residues (Lys453, Lys454, and Tyr455) are also involved in dimerization, but they are variable in this subfamily (Figure 1). In contrast, the interactions between the neighboring dimers are mediated by nonconserved residues with only 300–400 $Å^2$ of surface area buried at the interface (Figure 2f, right panel), consistent with the notion that the octamer forms through the tetramerization of the dimers. Indeed, the RMSD values of the four dimers are smaller than 0.1 Å. A square-shaped cavity with a side length of ~40 Å is found within the octamer with an entrance size of ~16 Å at the centers of the top and bottom tetramers (Figure S3). As the surface or the entrance of the cavity is not lined with conserved residues, it is unlikely that the cavity is related to the function of $LarA_{Bw}$.

2.3 | Production of $LarA_{Sp}$ in the holo state

To generate a LarAH in this subfamily in the holo state, we cloned the gene for a homolog of $LarA_{Bw}$ from *S. plurextorum*, a pathogen of swine, which shares

FIGURE 1 Multiple sequence alignment of LarA homologs (LarAHs) in a LarA subfamily with the second catalytic histidine residue substituted by an asparaginyl side chain. The catalytic histidine and the asparagine residues that are conserved in this subfamily are highlighted with red and purple stars, respectively. Other active site residues are indicated with green stars. Residues involved in the oligomerization are marked with orange stars and the lysine residue participating in covalent linkage with nickel-pincer nucleotide is labeled with a blue dot. The LarAH protein IDs and their respective species are listed below. HSR24722.1: *Candidatus* Eisenbacteria; HLG17431.1: *Blastocatellia*; HSB40499.1: *Candidatus* Methylomirabilota; MBM3218464.1: *Candidatus* Rokubacteria; MEW6533979.1: *Thermodesulfobacteriota*; RPJ22513.1: *Desulfobacteraceae*: MEC7736159.1: *Candidatus neomarinimicrobiota*; MFL2748578.1: Unidentified eubacterium; MDR5698079.1: *Candidatus* Caldifonticola tengchongensis; MEW6263215.1: *Thermodesulfobacteriota*.

1469896x, 2025, 12, Downloaded from https://onlinelibrary.wiley.com/doi/10.1002/pro.70362 by Universite Catholique De Louvain, Wiley Online Library on [13/11/2025]. See the Terms and Conditions (https://onlinelibrary.wiley.com/terms-and-conditions) on Wiley Online Library for rules of use; OA articles are governed by the applicable Creative Commons License

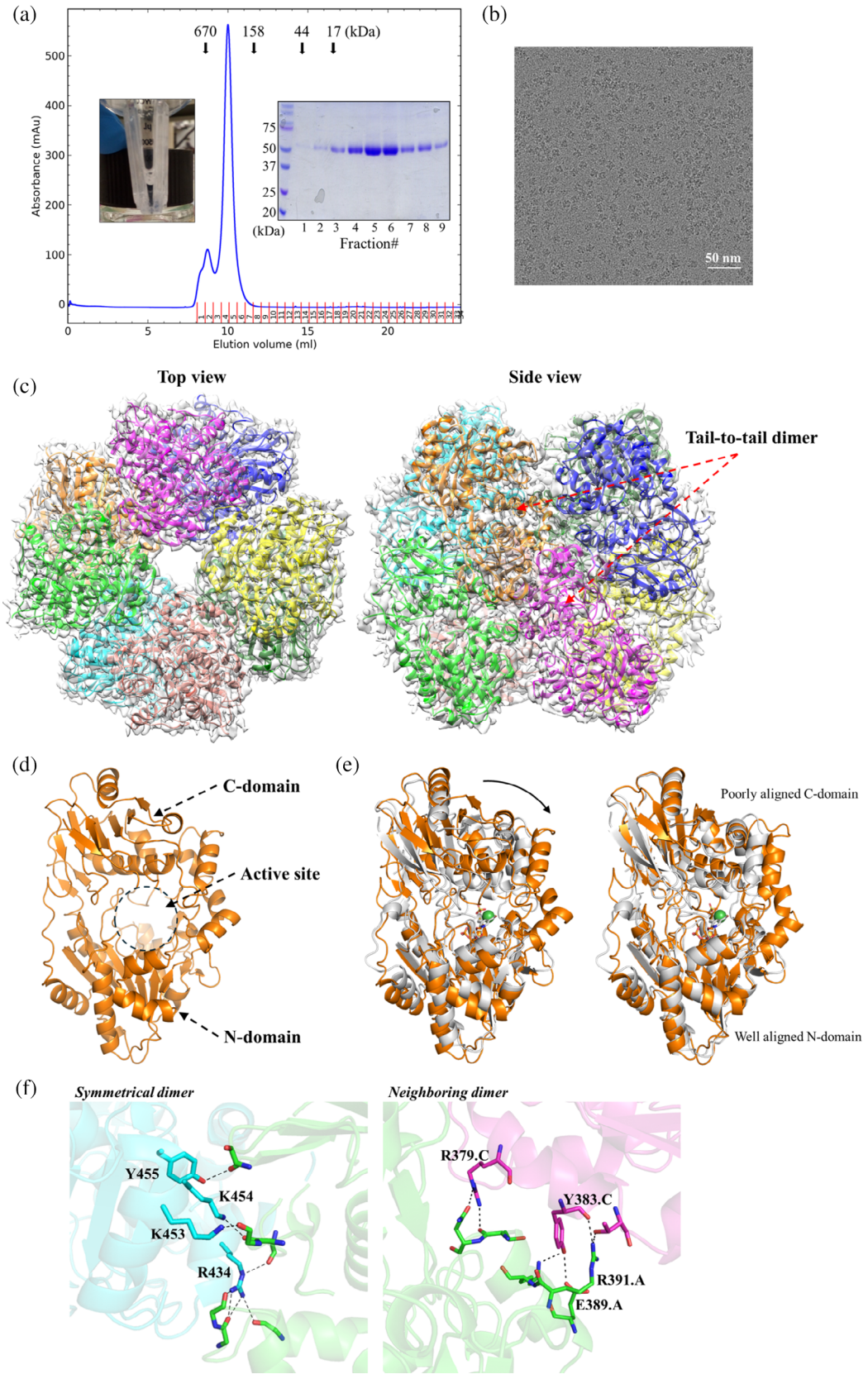


FIGURE 2 Legend on next page.

1469896x, 2025, 12, Downloaded from https://onlinelibrary.wiley.com/doi/10.1002/pro.70362 by Universite Catholique De Louvain, Wiley Online Library on [13/11/2025]. See the Terms and Conditions (https://onlinelibrary.wiley.com/terms-and-conditions) on Wiley Online Library for rules of use; OA articles are governed by the applicable Creative Commons License

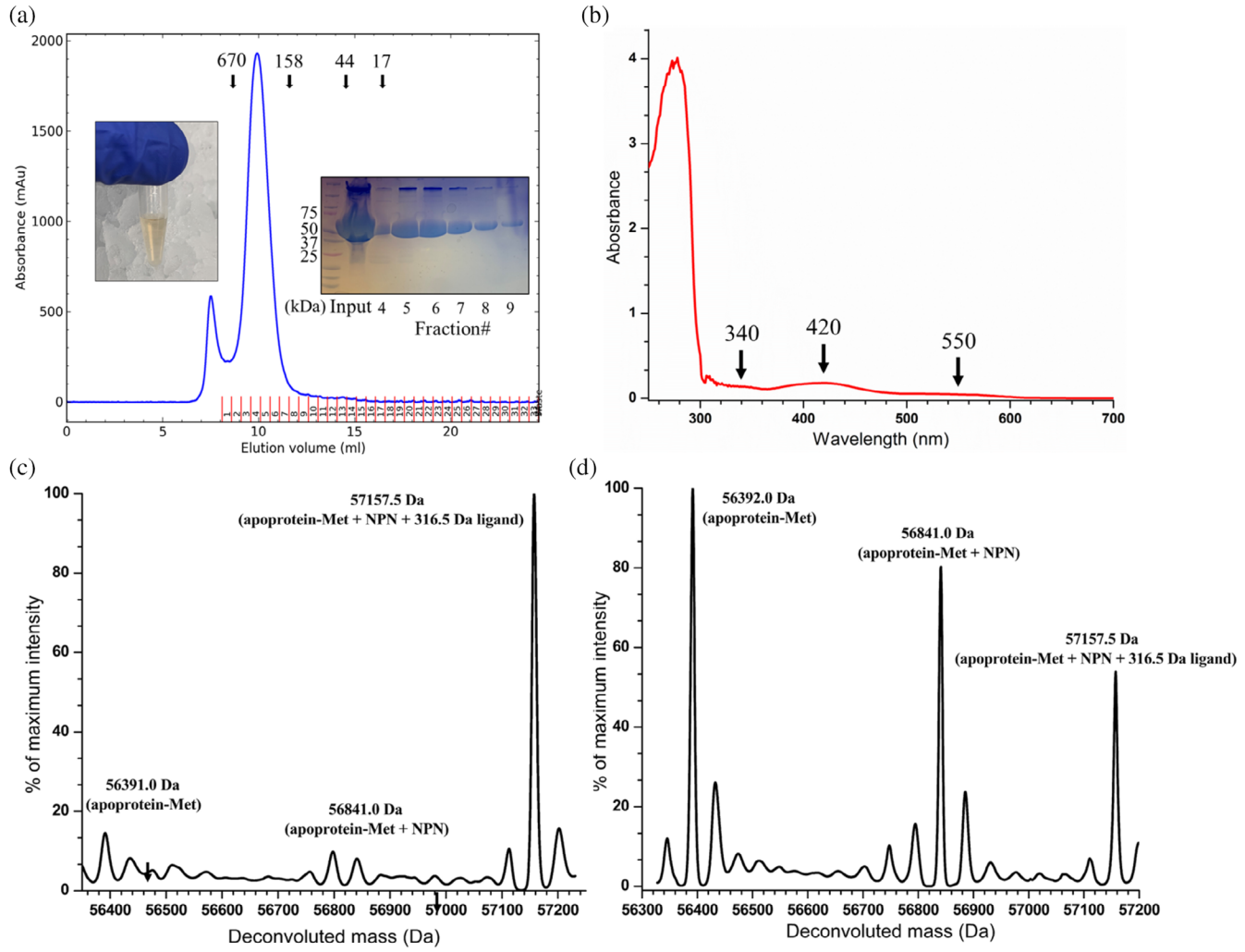


FIGURE 3 Production of LarAHs from *Streptococcus plurextorum* ($LarA_{Sp}$) in the holo state. (a) The size exclusion chromatography elution profile of $LarA_{Sp}$. The protein standards were eluted at the volumes indicated by the arrows. A photo of the purified and concentrated $LarA_{Sp}$ (~23 mg/mL) is shown in the left inset, and the sodium dodecyl sulfate–polyacrylamide gel electrophoresis profile of the peak fractions is shown in the right inset. (b) UV–visible spectrum of the purified $LarA_{Sp}$. The major absorption features are indicated with arrows. (c) and (d) electrospray ionization mass spectrometry analysis of purified $LarA_{Sp}$. The fresh sample is shown in (c) and an aged one is shown in (d). NPN, nickel-pincer nucleotide.

72% identical residues with $LarA_{Bw}$, and we co-expressed the C-terminal strep-tagged protein with LarB/C/D/E in *L. lactis*. The purified $LarA_{Sp}$ was eluted from SEC as a large oligomer with nearly the same apparent molecular weight as the octameric $LarA_{Bw}$ (Figure 3a). Importantly, the purified protein exhibited a

FIGURE 2 Cryo-electron microscopy (cryo-EM) structure of LarAHs from *Blautia wexlerae* ($LarA_{Bw}$). (a) The size exclusion chromatography elution profile of $LarA_{Bw}$. The protein standards, including thyroglobulin 670 kDa, gamma-globulin 158 kDa, ovalbumin 44 kDa, and myoglobulin 17 kDa, were eluted at the volumes indicated by the arrows. A photo of the purified and concentrated $LarA_{Bw}$ (~6 mg/mL) is shown in the left inset, and the sodium dodecyl sulfate–polyacrylamide gel electrophoresis profile of the peak fractions is shown in the right inset. (b) A representative cryo-EM micrograph of $LarA_{Bw}$. (c) Top view and side view of the octameric $LarA_{Bw}$ in the density map. The basic structural unit is the tail-to-tail dimer as indicated in the side view. (d) Structure of the monomeric $LarA_{Bw}$. The N- and C-domains of chain A, as well as the putative active site in between, are indicated. (e) Structural comparison of $LarA_{Bw}$ and LarA, from *Lactiplantibacillus plantarum* ($LarA_{Lp}$). *Left*: Structural superposition of $LarA_{Bw}$ (chain A, orange) and $LarA_{Lp}$ (5HUQ, chain B in gray). The nickel-pincer nucleotide cofactor in $LarA_{Lp}$ is shown in stick mode with the nickel depicted as a green sphere. The curved arrow indicates a more open conformation of $LarA_{Bw}$ in the apo state. *Right*: Structural superposition of separated N- and C-domains, revealing an overall good structural alignment for the N-domains but poor alignment for the C-domains. (f) Zoomed-in view of the interfaces stabilizing the octamer. *Left*: Polar contacts stabilizing the tail-to-tail dimerization. *Right*: Polar interactions between the neighboring subunits in a tetramer. Note that the conserved R434 is involved in multiple hydrogen bonds. Only the interfacial residues that use their side chains to form polar interactions are labeled and shown in stick mode. The polar interactions are indicated by dashed lines.

1469896x, 2025, 12, Downloaded from https://onlinelibrary.wiley.com/doi/10.1002/pro.70362 by Universite Catholique De Louvain, Wiley Online Library on [13/11/2025]. See the Terms and Conditions (https://onlinelibrary.wiley.com/terms-and-conditions) on Wiley Online Library for rules of use; OA articles are governed by the applicable Creative Commons License

yellow-brown color, which is consistent with the holo state of LarAHs. The UV–visible spectrum displayed weak absorptions at 340 and 550 nm, and a stronger absorption at 420 nm (Figure 3b). The absorptions at 420 and 550 nm are characteristic for the NPN cofactor-loaded LarAHs, whereas the absorption at 340 nm implies that a fraction of the purified protein may contain the reduced NPN cofactor, which was observed only when lactate (substrate) or $NaBH_4$ (hydride donor) was added to $LarA_{Lp}$ (Gatreddi et al., 2023; Rankin et al., 2018). These data imply that the purified $LarA_{Sp}$ may be bound with a ligand that putatively perturbs the redox state of the NPN cofactor.

Unexpectedly, electrospray ionization mass spectrometry (ESI-MS) analysis of the purified $LarA_{Sp}$ revealed a major species with a molecular weight of 57,157.5 Da (Figure 3c), which is 316.5 Da greater than the sum of the protein in the apo state (assuming loss of the N-terminal methionine residue, 56,392.0 Da) and the NPN cofactor (449.0 Da). Of interest, analysis of a sample stored at room temperature for 1 week showed that the major species degraded to the apo state protein and the holo state protein (i.e., the NPN cofactor-loaded state) (Figure 3d), suggesting that a covalently bound ligand with a molecular weight of 316.5 Da may be slowly released over time. Because the ESI-MS data demonstrated the holo state of the purified $LarA_{Sp}$, we were encouraged to move forward with structural characterization.

2.4 | Structure determination of $LarA_{Sp}$ in the holo state

The large molecular weight and C4 symmetry of $LarA_{Sp}$ allowed us to solve the cryo-EM structure of $LarA_{Sp}$ at a resolution of 2.2 Å (Figure 4a,b). Like $LarA_{Bw}$, $LarA_{Sp}$ also assembles as an octamer that is a tetrameric dimer, and the monomeric protein has a putative active site between the N- and C-domains (Figure 4c). Similar to $LarA_{Bw}$, a larger surface area (1130 $Å^2$) is buried at

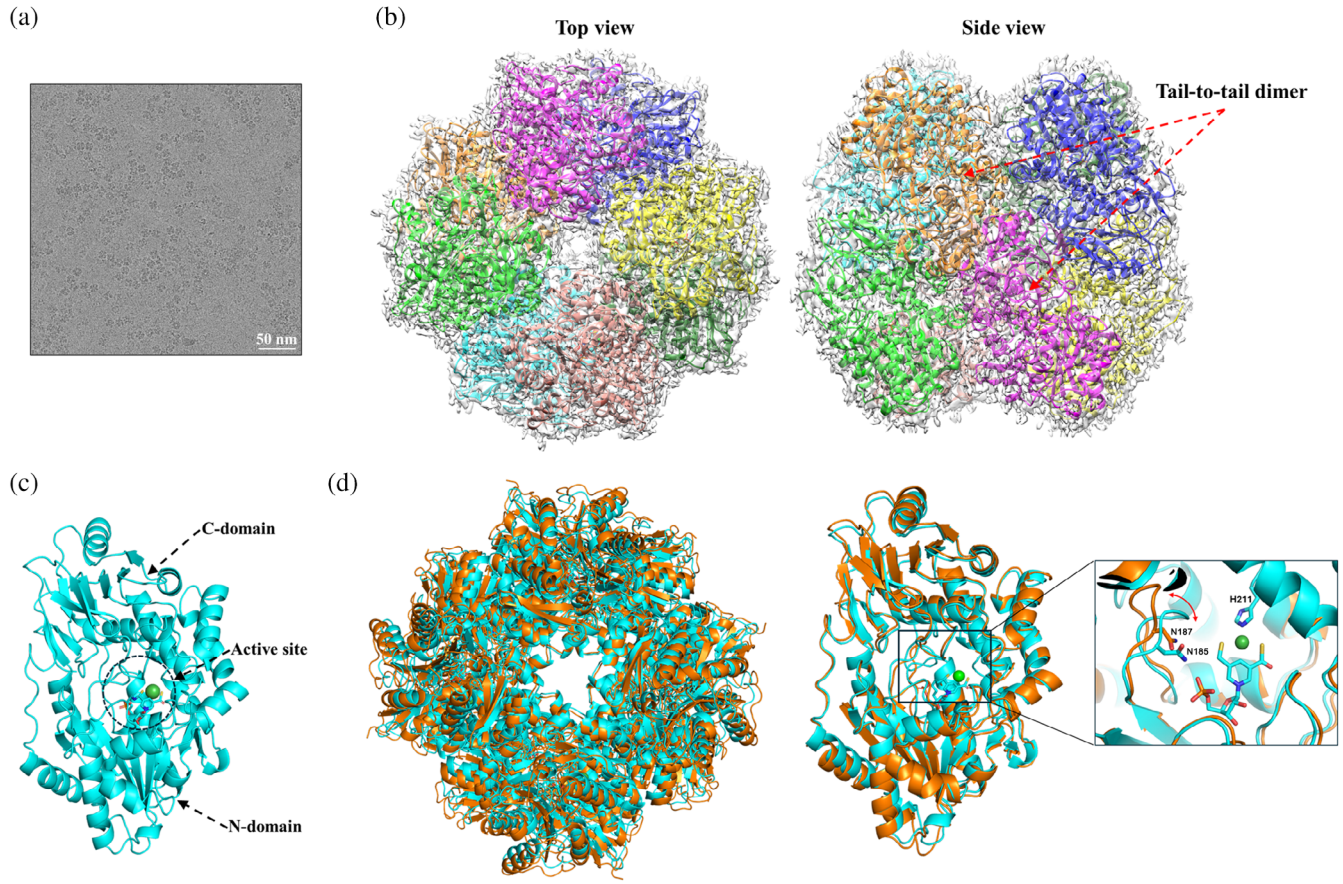


FIGURE 4 Cryo-electron microscopy (cryo-EM) structure of LarAHs from *Streptococcus plurextorum* ($LarA_{Sp}$). (a) A representative cryo-EM micrograph of $LarA_{Sp}$. (b) Top view and side view of the octameric $LarA_{Sp}$. (c) Structure of the monomeric $LarA_{Sp}$. The N- and C-domains of chain A, as well as the putative active site in between, are indicated. (d) Structural comparison of $LarA_{Sp}$ (cyan) and LarAHs from *Blautia wexlerae* ($LarA_{Bw}$) (orange). *Left*: Superposition of octamers. *Right*: Superposition of monomers. Insert: Zoomed-in view of the active site, highlighting the displacement of the loop containing the histidine-substituting asparagine residue with the red curve arrow. The nickel-pincer nucleotide cofactor and the asparagine residues are shown in stick mode and the nickel ion is depicted as a green sphere.

1469896x, 2025, 12, Downloaded from https://onlinelibrary.wiley.com/doi/10.1002/pro.70362 by Universite Catholique De Louvain, Wiley Online Library on [13/11/2025]. See the Terms and Conditions (https://onlinelibrary.wiley.com/terms-and-conditions) on Wiley Online Library for rules of use; OA articles are governed by the applicable Creative Commons License

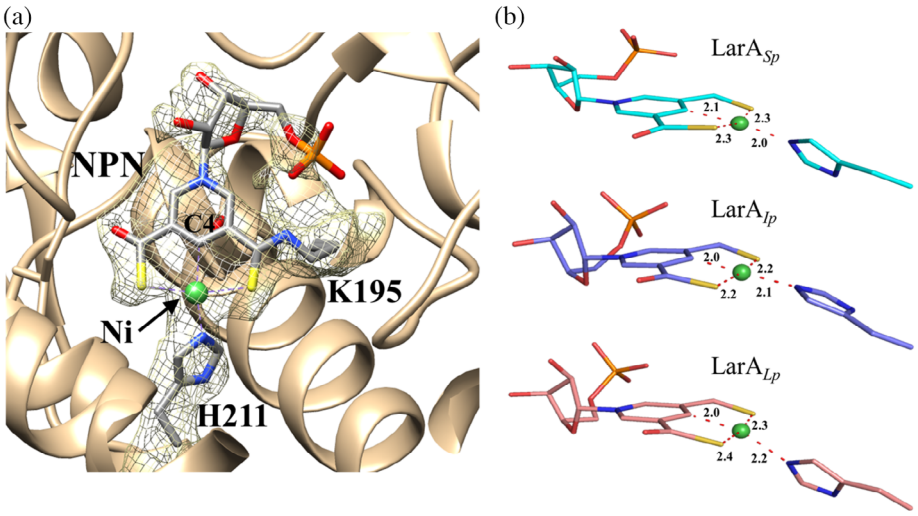


FIGURE 5 Nickel coordination in the nickel-pincer nucleotide (NPN) cofactor of LarAHs from *Streptococcus plurextorum* (LarA$_{Sp}$). (a) Cryo-electron microscopy density of the NPN cofactor (chain D) shown at a contour level of 0.0789. The density of the cofactor is connected to that of Lys195, indicating a thioamide bond. His211 is the fourth ligand that completes the distorted square-planar coordination of the nickel ion. (b) Comparison of Ni coordination in LarA$_{Sp}$, LarAH from *Isosphaera pallida* (LarA$_{Ip}$) (PDB 9EIA, chain A), and LarA from *Lactiplantibacillus plantarum* (LarA$_{Lp}$) (PDB 6C1W, chain B). The distances between Ni and coordinating atoms are labeled in angstroms.

the interface of two C-terminal domains than those between the neighboring monomers within the top or bottom tetramer (300–400 Å^2), supporting the notion that the basic unit of the octamer is a dimer. Arg431 (equivalent to Arg434 in LarA$_{Bw}$) forms multiple hydrogen bonds with the same set of residues from the other protomer as in LarA$_{Bw}$ at the dimerization interface, suggesting that the tail-to-tail dimer is common in this LarA subfamily whereas octamerization may not be so prevalent since the residues at the interface between the neighboring dimers are not conserved. The octameric LarA$_{Bw}$ and LarA$_{Sp}$ are highly superimposable with a Cα RMSD of 2.0 Å (Figure 4d, left panel), and the tail-to-tail dimers and monomers from both structures are aligned with the Cα RMSD values of 1.6 and 0.94 Å, respectively. Therefore, the loading of the NPN cofactor does not change the oligomerization or the domain orientation in each monomer, except that the loop containing the asparagine residue of interest moves toward the NPN cofactor in the holo state (Figure 4d, right panel). Ideally, we would compare the same protein in its apo and holo states. However, as we were unable to generate LarA$_{Bw}$ in its holo state and did not express LarA$_{Sp}$ in *E. coli* to produce the apo state protein, this direct comparison was not conducted in this study. Nevertheless, given the relatively high sequence identity between LarA$_{Bw}$ and LarA$_{Sp}$ (72%), the conclusion from this study would still be valid.

At the active site, a continuous density matches the NPN cofactor (Figure 5a). As this density is connected to the side chain of Lys195, the NPN cofactor forms a covalent linkage through a thioamide bond to the enzyme. Like in LarA$_{Lp}$ and LarA$_{lp}$, the nickel atom in the NPN cofactor is coordinated to the C4 atom of the pyridinium ring, two sulfur atoms, and the imidazole side chain of His211 in a square-planar coordination (Figure 5b). Over the NPN cofactor, we noticed electron density in close proximity to the conserved His115, His306, Tyr307, and His401, occupying a position corresponding to the substrate binding sites of other LarAHs (Figure S4). This density also extends toward the entrance of the active site. Considering the 340 nm absorption in the UV–visible spectrum (Figure 3b) and the 316.5 Da extra mass (Figure 3c,d), we speculate that an unidentified ligand is covalently bound at the substrate binding site. However, we were not successful in determining the identity of this ligand due to its low occupancy, as suggested by the poor density map. We also tried using mass spectrometry to identify the ligand, but were unable to obtain any meaningful information besides the molecular weight.

In parallel to the cryo-EM study, we also crystallized LarA$_{Sp}$ and solved the structure at 3.1 Å. Crystal packing analysis showed that LarA$_{Sp}$ forms the same octamer as revealed in the cryo-EM structure (Figure S5). The basic tail-to-tail dimers from the two octamers are highly superimposable with a Cα RMSD of 1.1 Å. However, due to the low resolution, the density in the x-ray structure was too poor to model the NPN cofactor or the unidentified ligand.

2.5 | Comparison of the active sites

The active sites of LarA$_{Sp}$ and LarA$_{Bw}$ were compared with those of LarA$_{lp}$ (Figure 6). Only a few residues in the active sites are conserved among these LarAHs.

1469896x, 2025, 12, Downloaded from https://onlinelibrary.wiley.com/doi/10.1002/pro.70362 by Universite Catholique De Louvain, Wiley Online Library on [13/11/2025]. See the Terms and Conditions (https://onlinelibrary.wiley.com/terms-and-conditions) on Wiley Online Library for rules of use; OA articles are governed by the applicable Creative Commons License

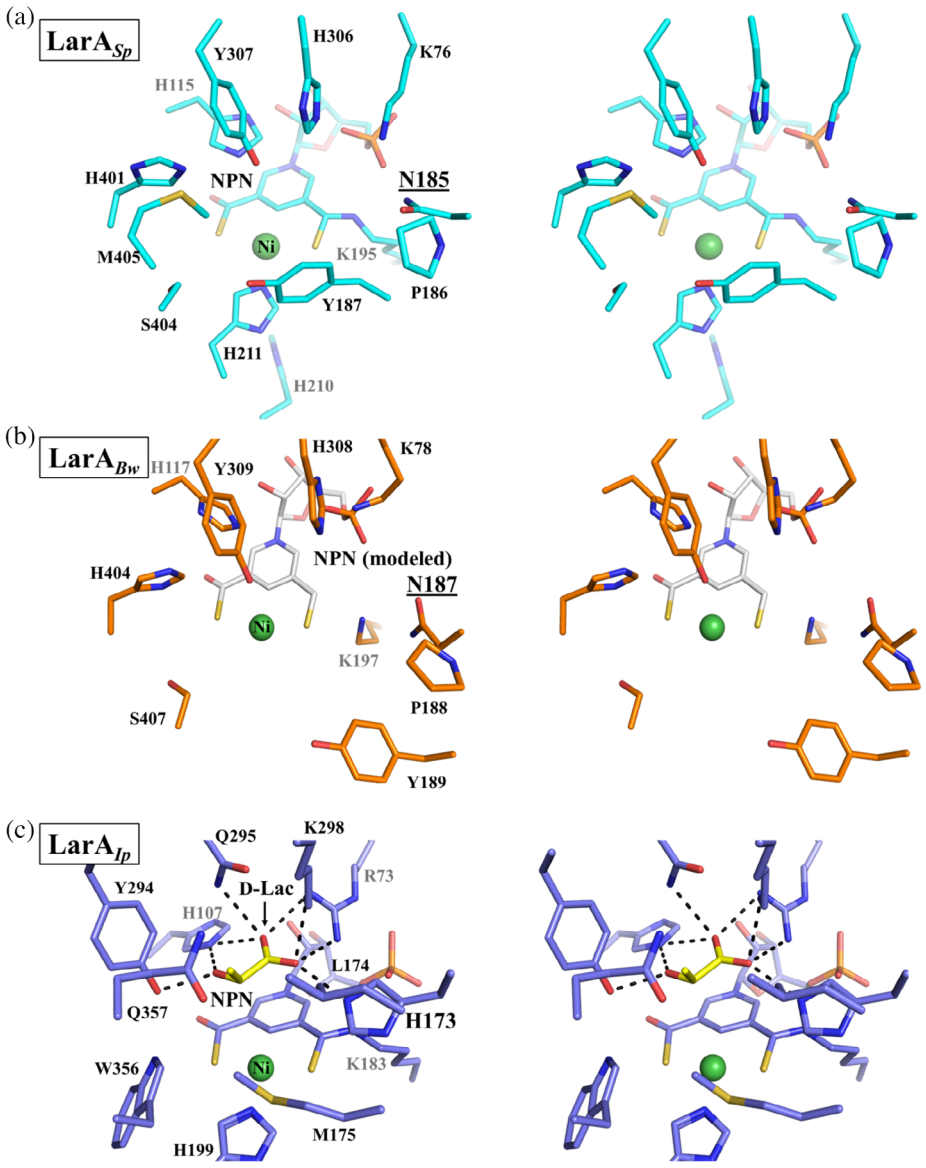


FIGURE 6 Stereo views of the active sites of (a) LarAHs from *Streptococcus plurextorum* (LarA$_{Sp}$) (cyan), (b) LarAHs from *Blautia wexlerae* (LarA$_{Bw}$) (orange), and (c) LarAH from *Isosphaera pallida* (LarA$_{Ip}$) (blue). LarA$_{Ip}$ (PDB 9EIA, chain A) is bound to an authentic substrate, D-lactate (D-Lac, yellow). Asn185 in LarA$_{Sp}$ and Asn187 in LarA$_{Bw}$, which substitute for the catalytic histidine residue in LarA$_{Ip}$ (His173), are underlined. An nickel-pincer nucleotide cofactor (white) is modeled in the structure of LarA$_{Bw}$ for better comparison. Some residues for nickel or substrate binding in LarA$_{Bw}$ were missing due to lack of electron density.

They include a catalytic histidyl side chain (His115, His117, and His107 in LarA$_{Sp}$, LarA$_{Bw}$, and LarA$_{Ip}$, respectively), the histidine residue for Ni coordination (His221, disordered His223, and His199), the lysyl group for the covalent linkage with the NPN cofactor (Lys195, Lys197, and Lys183), and the aspartate residue associating with the ribose moiety of the cofactor (Asp73, Asp75, and Asp70). In addition, Arg73 for the binding of the NPN phosphate group and the carboxylate group of D-lactate in LarA$_{Ip}$ is conservatively substituted with Lys76 in LarA$_{Sp}$ and Lys78 in LarA$_{Bw}$, respectively.

Besides these residues that are primarily involved in the binding of the NPN cofactor, other active site residues in LarA$_{Ip}$ are not identical to or conservatively substituted with those in the new subfamily members. The most notable difference is that the second catalytic histidyl group (His173 in LarA$_{Ip}$) is substituted by Asn185 in LarA$_{Sp}$ and Asn187 in LarA$_{Bw}$. According to the PCHT mechanism (Scheme 1), His107 and His173 in LarA$_{Ip}$ alternately function as a general base to deprotonate 2-OH of D/L-enantiomeric α-hydroxyacids and a general acid to protonate the pyruvate intermediate to complete racemization. Since the asparagine residue is absolutely conserved in the newly identified LarA subfamily (Figure 1) and topologically equivalent to the catalytic His173 in LarA$_{Ip}$ according to the structural comparison, its inability to catalyze an acid/base reaction rules out the possibility of functional equivalence to His173 in catalysis. Given that His107 and His173 deprotonate D- and L-enantiomers, respectively, the substitution of the L-enantiomer specific His173 with an asparagine residue suggests that LarA$_{Sp}$ and LarA$_{Bw}$ may only process D-enantiomer substrates and thus function as a unidirectional racemase/epimerase. Although uncommon, atypical racemases

1469896x, 2025, 12, Downloaded from https://onlinelibrary.wiley.com/doi/10.1002/pro.70362 by Universite Catholique De Louvain, Wiley Online Library on [13/11/2025]. See the Terms and Conditions (https://onlinelibrary.wiley.com/terms-and-conditions) on Wiley Online Library for rules of use; OA articles are governed by the applicable Creative Commons License

that process only one enantiomer have been reported. For instance, the cofactor independent aspartate/glutamate racemases usually use two cysteine residues to alternately act as a general base to deprotonate the chiral Cα to achieve racemization (Gallo & Knowles, 1993; Yamauchi et al., 1992). Remarkably, some aspartate/glutamate racemases have only one cysteine residue with the other replaced by a non-cysteine residue. Biochemical and structural studies of such an enzyme from *E. coli* showed that it only catalyzes the conversion from an L-amino acid to a D-amino acid but cannot catalyze the D-to-L conversion, which has been attributed to the lack of the second catalytic cysteine residue (Ahn et al., 2015). In addition to the lack of the catalytic histidine residue, many other active site residues of $LarA_{Sp}$ and $LarA_{Bw}$ are different from those in $LarA_{lp}$ (Figure 6), strongly suggesting that these putative enzymes may process chemicals that are very different from the known substrates of LarAs. Consistently, we were unable to detect any racemization activity of $LarA_{Sp}$ for D-/L-lactate (data not shown), likely at least in part due to the presence of a single histidine residue at the active site, whereas it has been shown that many promiscuous LarAHs are able to process lactate (Gatreddi et al., 2025; Urdiain-Arraiza et al., 2025).

2.6 | Potential involvement in carbohydrate metabolism

Genomic context analysis can facilitate identifying substrates of enzymes (Zhao et al., 2014), including LarAHs (Desguin et al., 2020). In this work, we examined the contexts of the genes encoding $LarA_{Sp}$ and $LarA_{Bw}$, respectively. Of interest, both *larA* genes have gene neighbors that potentially encode enzymes involved in glycolysis, including glucose-6-phosphate isomerase, fructose-6-phosphate-1-phosphotransferase and triose phosphate isomerase in *S. plurextorum*, and fructose-1,-6-bisphosphatase, triose phosphate isomerase, fructose-bisphosphate aldolase, glucosamine-6-phosphate isomerase, and aldolase-1-epimerase in *B. wexlerae* (Figure S6). Several genes encoding subfamily members that share sequence identity as low as 37% (Figure 1) are also located next to the genes encoding possible sugar ATP-binding cassette transporters and enzymes involved in carbohydrate metabolism, allowing us to speculate that these LarAHs are potential carbohydrate-processing enzymes. Based on the density map and the MS data, we modeled a linear phosphorylated aldose with a formula of $C_9H_{19}O_{10}P$ (316.2 Da for the deprotonated form) to fit the density (Figure S7). Although this model is highly speculative, it suggests the size and shape of this unidentified ligand.

3 | CONCLUSION

In this study, we characterized two members of a newly identified LarA subfamily that lacks one of the catalytic histidine residues conserved in other LarAHs. Using cryo-EM, we determined their structures in the apo and holo states at atomic resolutions. From the structural data, combined with MS and spectroscopic analysis, as well as genomic context analysis, our findings revealed (1) a unique octameric assembly, which is unprecedented among other known LarAHs; (2) a distinct set of active site residues, including the asparagine side chain substitution for the missing histidyl group, suggesting recognition and processing of non-canonical LarA substrates; and (3) genomic and structural evidence hypothetically linking these LarAHs to carbohydrate metabolism. This work provides a foundation for exploring the biological functions and catalytic mechanisms of these putative enzymes potentially involved in carbohydrate metabolism.

4 | METHODS

4.1 | Genes and constructs

To express $LarA_{Bw}$ in *L. lactis*, a *Pci*I restriction enzyme site was first introduced into the pGIR112 vector (Desguin et al., 2015) using primers PciI_F and PciI_R, and then the polymerase chain reaction (PCR) product of the gene encoding $LarA_{Bw}$ amplified using primers LarAH13_F and LarAH13_R was inserted into the plasmid via *Pci*I and *Nhe*I, generating the plasmid pGIR112_$LarA_{Bw}$. The gene encoding $LarA_{Sp}$ was PCR amplified using primers LarAH37_A and LarAH37_B2, digested by *Xba*I and *Pci*I, and inserted into the pGIR210 vector (Desguin et al., 2020) that had been digested with *Nhe*I and *Pci*I, generating the plasmid pGIR213 for co-expression of $LarA_{Sp}$ with LarB/C/E in *Lactococcus lactis*. The plasmids and primers used in this study are listed in Table S1.

4.2 | Protein expression and purification

Expression and purification of $LarA_{Bw}$. The *E. coli* strain BL21-Gold(DE3) bearing the pET23b plasmid expressing $LarA_{Bw}$ (Chatterjee et al., 2016) was grown overnight at 37°C and 220 rpm in lysogeny broth (LB) containing 100 μg/mL of ampicillin. The overnight grown culture was diluted to 1% with LB broth supplemented with 100 μg/mL of ampicillin and allowed to grow at 37°C with shaking at 220 rpm. When the optical density at 600 nm (OD_{600}) reached 0.35, the culture was cold-shocked by incubating on ice for 20 min and then 0.1 mM isopropyl β-D-1-thiogalactopyranoside

1469896x, 2025, 12, Downloaded from https://onlinelibrary.wiley.com/doi/10.1002/pro.70362 by Universite Catholique De Louvain, Wiley Online Library on [13/11/2025]. See the Terms and Conditions (https://onlinelibrary.wiley.com/terms-and-conditions) on Wiley Online Library for rules of use; OA articles are governed by the applicable Creative Commons License

was added, followed by shaking at 16°C for 24 h. Cells were harvested by centrifugation at 6000 rpm for 10 min. Pelleted cells were resuspended in a buffer containing 20 mM Tris, pH 8.0, 300 mM NaCl, and 5% glycerol. Cells were lysed by sonication and the supernatant was collected after centrifugation at 20,000 *g* and 4°C for 35 min. His_6-tagged $LarA_{Bw}$ in the supernatant was sequentially purified using the Nickel-nitrilotriacetic acid resin and then a Superdex 200 increase 10/300 GL column equilibrated with a buffer containing 10 mM 4-(2-hydroxyethyl)-1-piperazineethanesulfonic acid, pH 7.8, and 150 mM NaCl. The peak fractions from SEC were pooled for cryo-EM grid preparation.

Expression and purification of $LarA_{Sp}$. The *Lactococcus lactis* cells transformed with the pGIR213 plasmid were grown without shaking at 30°C overnight in M17 media supplemented with 0.5% glucose and 7.5 μg/mL of chloramphenicol. The overnight-grown culture was diluted to 1% with M17 medium containing 0.5% glucose and 7.5 μg/mL of chloramphenicol and grown at 30°C with gentle shaking at 40 rpm until the OD_{600} reached 0.4–0.5. Protein expression was induced by adding 5 μg of Nisin A per liter culture for 4 h, after which the culture was stationed overnight at 4°C before cell harvest by centrifugation at 4000 *g* for 20 min. Pelleted cells were resuspended in a buffer containing 100 mM Tris, pH 7.5, 150 mM NaCl, 2.5 μg/mL of *DNase* I, and 15 μg/mL of lysozyme. Cell lysis was performed using a French Press at 15,000 psi by passing the cell suspension twice. Clarified supernatant was obtained after centrifugation at 18,000 *g* and 4°C for 1 h and applied to Strep-Tactin®XT 4Flow® high-capacity resin (IBA Lifesciences) pre-equilibrated with a buffer containing 100 mM Tris, pH 7.5, and 150 mM NaCl. Resin was washed with 100 mM Tris, pH 7.5, and 150 mM NaCl, and strep-tagged $LarA_{Sp}$ was eluted with the wash buffer supplemented with 50 mM biotin. The elution fractions containing the protein of interest were concentrated using an Amicon Ultra centrifugal filter and then applied to a Superdex 200 increase 10/300 GL column. The peak fractions from SEC were pooled for cryo-EM grid preparation and crystallization within 24 h.

4.3 | UV–visible spectroscopy

The UV–visible spectrum (250–700 nm) of purified $LarA_{Sp}$ (23 mg/mL) was recorded on a Shimadzu UV-2600 spectrophotometer (Kyoto, Japan) with a 10 mm path length and a 2 nm slit width for two accumulations.

4.4 | ESI-MS analysis

Purified $LarAH_{Sp}$ in 50 mM Tris, pH 7.5, and 125 mM NaCl was analyzed by ESI-MS. Data were collected in positive ion mode on a Xevo G2-XS QTof (Waters) equipped with a Thermo Hypersil Gold CN guard desalting column. Ten microliters of protein sample was injected at a flow rate of 0.1 mL/min. The mobile phases were 0.1% formic acid in water (solvent A) and acetonitrile (solvent B) initially mixed at a 98%:2% ratio, and then solvent B was gradually increased to 75%. The MaxEnt1 algorithm was used to generate the molecular mass spectra.

4.5 | Cryo-EM grid preparation, data collection, and processing

Quantifoil R2/2 UT 200 mesh copper grids (for $LarA_{Bw}$) or Quantifoil R1.2/1.3200 mesh copper grids (for $LarA_{Sp}$) were treated using a Pelco easiGlow™ glow discharge for 45 s. Five microliters of the sample at 2 mg/mL (for $LarA_{Bw}$) or 3.5 μL of the sample at 1.5 mg/mL (for $LarA_{Sp}$) was added to the grid. The grids were then blotted using a Vitrobot Mark IV system before being plunged into liquid ethane.

For $LarA_{Bw}$, single particle cryo-EM data were collected at the Cryo-EM facility of Michigan State University using a Talos Arctica equipped with a Falcon 3 direct electron detector, operating at 200 keV. A total of 1539 micrographs were collected at ×120,000 nominal magnification (0.872 Å/pixel) over 44.60 s for a total dose of 32.27 $e^-/Å^2$. For $LarA_{Sp}$, single particle cryo-EM data were collected using the Talos Arctica equipped with a Falcon 4i direct electron detector, operating at 200 keV with a post-column Selectris energy filter (10-eV slit width). A total of 4657 micrographs were collected at ×130,000 nominal magnification (0.886 Å/pixel) in Electron Event Representation (EER) format over 6.0 s for a total dose of 44.71 $e^-/Å^2$.

The data were processed using CryoSPARC (Punjani et al., 2017). Briefly, the micrographs were first motion corrected using patch motion correction, followed by contrast transfer function (CTF) estimation using patch CTF estimation, and particles were picked using a blob picker followed by template picking. For $LarA_{Bw}$, a total of 219,896 particles were used for 3D refinement with C4 symmetry. For $LarA_{Sp}$, a total of 571,110 particles were used for 3D refinement with C4 symmetry. The overall resolution was estimated based on the gold-standard Fourier shell correlation ($FSC_{0.143}$) (Henderson et al., 2012). The final maps were deposited into the Electron Microscopy Data Bank (EMDB). The data processing procedures are described in Figure S8 for $LarA_{Bw}$ and Figure S9 for $LarA_{Sp}$. Initial models were generated using ModelAngelo in sequence mode (Jamali et al., 2024). Refinement was carried out using Phenix (Liebschner et al., 2019), and model adjustments were carried out in Coot (Emsley et al., 2010). Residues 4–211, 233–407, and 412–480 and residues 2–481 were modeled in the

1469896x, 2025, 12, Downloaded from https://onlinelibrary.wiley.com/doi/10.1002/pro.70362 by Universite Catholique De Louvain, Wiley Online Library on [13/11/2025]. See the Terms and Conditions (https://onlinelibrary.wiley.com/terms-and-conditions) on Wiley Online Library for rules of use; OA articles are governed by the applicable Creative Commons License

structures of $LarA_{Bw}$ and $LarA_{Sp}$, respectively. Model parameters were monitored using MolProbity in Phenix, and the values are listed in Table S2 along with the respective Electron Microscopy Data (EMD) and PDB IDs. Representative density maps of both proteins are shown in Figure S10.

4.6 | Crystallization and structure determination of $LarA_{Sp}$

The peak fractions from SEC were concentrated to 19 mg/mL for crystallization screening. Crystals were obtained at 21°C with a reservoir buffer containing 0.49M sodium phosphate monobasic monohydrate and 0.91M potassium phosphate dibasic, pH 6.9 and flash frozen in liquid nitrogen.

The diffraction data were collected at the National Synchrotron Light Source II (NSLS-II) of Brookhaven National Laboratory on the 17-ID-2 (FMX) beamline. The dataset was indexed, integrated, and scaled using X-ray Detector Software from the FastDP pipeline at NSLS-II. Molecular replacement was performed to solve the structure using a monomer from the cryo-EM structure as the search model. Refinement was performed using Phenix.refine and the model was built using Coot iteratively. Crystallographic statistics are listed in Table S3.

AUTHOR CONTRIBUTIONS

Santhosh Gatreddi: Investigation; data curation; formal analysis; validation; visualization; writing – original draft; writing – review and editing. **Sundharraman Subramanian:** Investigation; validation; formal analysis; data curation; writing – original draft; writing – review and editing; visualization. **Dexin Sui:** Investigation; validation. **Tianqi Wang:** Investigation; validation; writing – original draft. **Julian Urdiain-Arraiza:** Investigation; validation; formal analysis; data curation; writing – original draft. **Benoît Desguin:** Conceptualization; investigation; funding acquisition; writing – original draft; writing – review and editing; supervision; resources; data curation; formal analysis; project administration. **Robert P. Hausinger:** Conceptualization; funding acquisition; writing – original draft; investigation; formal analysis; supervision; data curation; visualization; project administration; resources; writing – review and editing. **Kristin N. Parent:** Conceptualization; investigation; funding acquisition; visualization; writing – review and editing; formal analysis; project administration; data curation; supervision; resources. **Jian Hu:** Conceptualization; data curation; visualization; funding acquisition; project administration; supervision; resources; writing – original draft; writing – review and editing; investigation; formal analysis.

ACKNOWLEDGMENTS

We thank Prof. Dennis W. Wolan for providing us with plasmid pET23b expressing $LarA_{BW}$. We thank the MSU RTSF Cryo-EM Core Facility for data collection and processing. We thank the 17-ID-2 beamline scientist in NSLS-II for diffraction data collection and processing. This work was supported by National Institutes of Health GM128959 (to Robert P. Hausinger and Jian Hu), GM128959 (to Robert P. Hausinger), GM140931 (to Jian Hu), GM140803 (to Kristin N. Parent) and the UCLouvain Fonds Spécial de Recherche (to Benoît Desguin).

CONFLICT OF INTEREST STATEMENT

The authors declare no competing interests.

DATA AVAILABILITY STATEMENT

For cryo-EM structures, the density maps and corresponding atomic models have been deposited in the Electron Microscopy Data Bank (EMD-72199 for $LarA_{Bw}$ and EMD-72200 for $LarA_{Sp}$) and PDB (9Q3J and 9Q3K), respectively. The atomic coordinates and structure factors of the crystal structure of $LarA_{Sp}$ have been deposited in the PDB with the access code of 9Q2U. All data needed to evaluate the conclusions in the paper are present in the main text and/or in Supporting Information S1. Additional data related to this paper may be requested from the corresponding authors.

ORCID

Jian Hu https://orcid.org/0000-0001-6657-9826

REFERENCES

Ahn J-W, Chang JH, Kim K-J. Structural basis for an atypical active site of an l-aspartate/glutamate-specific racemase from *Escherichia coli*. FEBS Lett. 2015;589:3842–7. https://doi.org/10.1016/j.febslet.2015.11.003

Cantwell A, Dennis D. Lactate racemase. Direct evidence for an α-carbonyl intermediate. Biochemistry. 1974;13:287–91. https://doi.org/10.1021/bi00699a009

Chatterjee S, Gatreddi S, Gupta S, Nevarez JL, Rankin JA, Turmo A, et al. Unveiling the mechanisms and biosynthesis of a novel nickel-pincer enzyme. Biochem Soc Trans. 2022;50:1187–96. https://doi.org/10.1042/BST20220490

Chatterjee S, Nevarez JL, Rankin JA, Hu J, Hausinger RP. Structure of the LarB–substrate complex and identification of a reaction intermediate during nickel-pincer nucleotide cofactor biosynthesis. Biochemistry. 2023;62:3096–104. https://doi.org/10.1021/acs.biochem.3c00242

Chatterjee S, Parson KF, Ruotolo BT, McCracken J, Hu J, Hausinger RP. Characterization of a [4Fe-4S]-dependent LarE sulfur insertase that facilitates nickel-pincer nucleotide cofactor biosynthesis in *Thermotoga maritima*. J Biol Chem. 2022;298:102131. https://doi.org/10.1016/j.jbc.2022.102131

Chatterjee S, Stupp GS, Park SKR, Ducom J-C, Yates JR, Su AI, et al. A comprehensive and scalable database search system for metaproteomics. BMC Genomics. 2016;17:642. https://doi.org/10.1186/s12864-016-2855-3

Desguin B, Fellner M, Riant O, Hu J, Hausinger RP, Hols P, et al. Biosynthesis of the nickel-pincer nucleotide cofactor of lactate racemase requires a CTP-dependent cyclometallase. J Biol Chem. 2018;293:12303–17. https://doi.org/10.1074/jbc.RA118.003741

Desguin B, Goffin P, Viaene E, Kleerebezem M, Martin-Diaconescu V, Maroney MJ, et al. Lactate racemase is a nickel-dependent enzyme activated by a widespread maturation

1469896x, 2025, 12, Downloaded from https://onlinelibrary.wiley.com/doi/10.1002/pro.70362 by Universite Catholique De Louvain, Wiley Online Library on [13/11/2025]. See the Terms and Conditions (https://onlinelibrary.wiley.com/terms-and-conditions) on Wiley Online Library for rules of use; OA articles are governed by the applicable Creative Commons License

system. Nat Commun. 2014;5:3615. https://doi.org/10.1038/ncomms4615
Desguin B, Soumillion P, Hols P, Hausinger RP. Nickel-pincer cofactor biosynthesis involves LarB-catalyzed pyridinium carboxylation and LarE-dependent sacrificial sulfur insertion. Proc Natl Acad Sci U S A. 2016;113:5598–603. https://doi.org/10.1073/pnas.1600486113
Desguin B, Urdiain-Arraiza J, Da Costa M, Fellner M, Hu J, Hausinger RP, et al. Uncovering a superfamily of nickel-dependent hydroxyacid racemases and epimerases. Sci Rep. 2020;10:18123. https://doi.org/10.1038/s41598-020-74802-6
Desguin B, Zhang T, Soumillion P, Hols P, Hu J, Hausinger RP. A tethered niacin-derived pincer complex with a nickel-carbon bond in lactate racemase. Science. 2015;349:66–9. https://doi.org/10.1126/science.aab2272
Emsley P, Lohkamp B, Scott WG, Cowtan K. Features and development of Coot. Acta Crystallogr D Biol Crystallogr. 2010;66:486–501. https://doi.org/10.1107/s0907444910007493
Fellner M, Desguin B, Hausinger RP, Hu J. Structural insights into the catalytic mechanism of a sacrificial sulfur insertase of the N-type ATP pyrophosphatase family, LarE. Proc Natl Acad Sci U S A. 2017;114:9074–9. https://doi.org/10.1073/pnas.1704967114
Fellner M, Rankin JA, Desguin B, Hu J, Hausinger RP. Analysis of the active site cysteine residue of the sacrificial sulfur insertase LarE from *Lactobacillus plantarum*. Biochemistry. 2018;57:5513–23. https://doi.org/10.1021/acs.biochem.8b00601
Gallo KA, Knowles JR. Purification, cloning, and cofactor independence of glutamate racemase from *Lactobacillus*. Biochemistry. 1993;32:3981–90. https://doi.org/10.1021/bi00066a019
Gatreddi S, Sui D, Hausinger RP, Hu J. Irreversible inactivation of lactate racemase by sodium borohydride reveals reactivity of the nickel–pincer nucleotide cofactor. ACS Catal. 2023;13:1441–8.
Gatreddi S, Urdiain-Arraiza J, Desguin B, Hausinger RP, Hu J. Structural and mutational characterization of a malate racemase from the LarA superfamily. Biometals. 2022;36:303–13. https://doi.org/10.1007/s10534-022-00372-x
Gatreddi S, Urdiain-Arraiza J, Desguin B, Hausinger RP, Hu J. Structural basis for the catalysis and substrate specificity of a LarA racemase with a broad substrate spectrum. ACS Catal. 2025;15:2857–66. https://doi.org/10.1021/acscatal.4c07804
Hausinger RP, Desguin B, Fellner M, Rankin JA, Hu J. Nickel–pincer nucleotide cofactor. Curr Opin Chem Biol. 2018;47:18–23. https://doi.org/10.1016/j.cbpa.2018.06.019
Henderson R, Sali A, Baker ML, Carragher B, Devkota B, Downing KH, et al. Outcome of the first electron microscopy validation task force meeting. Structure. 2012;20:205–14. https://doi.org/10.1016/j.str.2011.12.014
Hiyama T, Fukui S, Kitahara K. Purification and properties of lactate racemase from *Lactobacillus sake*. J Biochem. 1968;64:99–107. https://doi.org/10.1093/oxfordjournals.jbchem.a128870
Jamali K, Käll L, Zhang R, Brown A, Kimanius D, Scheres SHW. Automated model building and protein identification in cryo-EM maps. Nature. 2024;628:450–7. https://doi.org/10.1038/s41586-024-07215-4
Katagiri H, Sugimori T, Imai K, Komaki S, Okuzumi M, Anyoji H. On the metabolism of organic acids by *Clostridium acetobutylicum*. Agric Biol Chem. 1961;25:281–313. https://doi.org/10.1080/00021369.1961.10857808
Liebschner D, Afonine PV, Baker ML, Bunkóczi G, Chen VB, Croll TI, et al. Macromolecular structure determination using X-rays, neutrons and electrons: recent developments in Phenix. Acta Crystallogr D Struct Biol. 2019;75:861–77. https://doi.org/10.1107/s2059798319011471
Nevarez JL, Turmo A, Gatreddi S, Gupta S, Hu J, Hausinger RP. Overcoming barriers for investigating nickel-pincer nucleotide cofactor-related enzymes. mBio. 2024;16:e0340424. https://doi.org/10.1128/mbio.03404-24
Punjani A, Rubinstein JL, Fleet DJ, Brubaker MA. cryoSPARC: algorithms for rapid unsupervised cryo-EM structure determination. Nat Methods. 2017;14:290–6. https://doi.org/10.1038/nmeth.4169
Rankin JA, Chatterjee S, Tariq Z, Lagishetty S, Desguin B, Hu J, et al. The LarB carboxylase/hydrolase forms a transient cysteinyl-pyridine intermediate during nickel-pincer nucleotide cofactor biosynthesis. Proc Natl Acad Sci U S A. 2021;118:e2106202118. https://doi.org/10.1073/pnas.2106202118
Rankin JA, Mauban RC, Fellner M, Desguin B, McCracken J, Hu J, et al. Lactate racemase nickel-pincer cofactor operates by a proton-coupled hydride transfer mechanism. Biochemistry. 2018;57:3244–51. https://doi.org/10.1021/acs.biochem.8b00100
Shapiro SS, Dennis D. Lactic acid racemization in *Clostridium butylicum*. Evidence for a direct internal hydride shift. Biochemistry. 1965;4:2283–8. https://doi.org/10.1021/bi00887a004
Turmo A, Hu J, Hausinger RP. Characterization of the nickel-inserting cyclometallase LarC from *Moorella thermoacetica* and identification of a cytidinylylated reaction intermediate. Metallomics. 2022;14:mfac014. https://doi.org/10.1093/mtomcs/mfac014
Urdiain-Arraiza J, Vandenberghe A, Dimitrova G, Desguin B. Unveiling 14 novel 2-hydroxy acid racemization and epimerization reactions in the lactate racemase superfamily. J Biol Chem. 2025;301:108069. https://doi.org/10.1016/j.jbc.2024.108069
Yamauchi T, Choi SY, Okada H, Yohda M, Kumagai H, Esaki N, et al. Properties of aspartate racemase, a pyridoxal 5′-phosphate-independent amino acid racemase. J Biol Chem. 1992;267:18361–4. https://doi.org/10.1016/s0021-9258(19)36969-8
Zhao S, Sakai A, Zhang X, Vetting MW, Kumar R, Hillerich B, et al. Prediction and characterization of enzymatic activities guided by sequence similarity and genome neighborhood networks. elife. 2014;3:e03275. https://doi.org/10.7554/eLife.03275

SUPPORTING INFORMATION

Additional supporting information can be found online in the Supporting Information section at the end of this article.

How to cite this article: Gatreddi S, Subramanian S, Sui D, Wang T, Urdiain-Arraiza J, Desguin B, et al. Structures of two LarA-like nickel-pincer nucleotide cofactor-utilizing enzymes with a single catalytic histidine residue. Protein Science. 2025;34(12):e70362. https://doi.org/10.1002/pro.70362

1469896x, 2025, 12, Downloaded from https://onlinelibrary.wiley.com/doi/10.1002/pro.70362 by Universite Catholique De Louvain, Wiley Online Library on [13/11/2025]. See the Terms and Conditions (https://onlinelibrary.wiley.com/terms-and-conditions) on Wiley Online Library for rules of use; OA articles are governed by the applicable Creative Commons License